Acta Scientiarum

http://www.uem.br/acta
ISSN printed: 1806-2563
ISSN on-line: 1807-8664
Doi: 10.4025/actascitechnol.v36i2.17995

Effect of Pr_6O_{11} doping in electrical and microstructural properties of SnO_2-based varistors

Hervê Stangler Irion, Eder Carlos Ferreira de Souza, André Vitor Chaves de Andrade, Sandra Regina Masetto Antunes and Augusto Celso Antunes*

*Departamento de Química, Universidade Estadual de Ponta Grossa, Av. Carlos Cavalcanti, 4748, 84030-900, Ponta Grossa, Paraná, Brazil. *Author for correspondence. E-mail: augusto.celso@pq.cnpq.br*

ABSTRACT. The influence of the dopant Pr_6O_{11} was investigated with regard to the electrical and microstructural properties of the system $(98.95\text{-}x)\%SnO_2.1.0\%CoO.0.05\%Ta_2O_5.x\%Pr_6O_{11}$, where x = 0.05%, 0.10%, 0.30% and 0.50% in mol. Pr_6O_{11} doping modifies the electrical behavior of the ceramics. The electrical parameters were: α = 8.0, E_B = 319 V cm^{-1} and V_b = 0.66 V $barrier^{-1}$ for the system without Pr_6O_{11} and α = 17.0, E_B = 853 V cm^{-1} and V_b = 1.15 V $barrier^{-1}$ with the addition of 0.10% in mol Pr_6O_{11}. The system with 0.05% in mol Pr_6O_{11} had the same non-linearity coefficient α as the system with 0.10% in mol. However, breakdown electrical field and voltage per barrier rates were lower (E_B = 708 V cm^{-1} and V_b = 0.98 V $barrier^{-1}$). The low rates in the breakdown electrical field enabled the varistor systems under study to be used in protection systems for low-voltage energy grids. In the case of Pr_6O_{11} concentrations above 0.10% in mol, the presence of the dopant became deleterious to the varistor's electrical characteristics. This effect was due to an increase in praseodymium stannate ($Pr_2Sn_2O_7$) secondary phase. The crystalline phase coupled to the cassiterite (SnO_2) phase was found with XRD and SEM/EDS and quantified by Rietveld's refining method.

Keywords: characterization, tin dioxide, praseodymium oxide, tantalum oxide.

Efeito da dopagem com Pr_6O_{11} nas propriedades elétricas e microestruturais de varistores a base de SnO_2

RESUMO. Neste trabalho foi investigada a influência do dopante Pr_6O_{11} nas propriedades elétricas e microestruturais do sistema $(98{,}95\text{-}x)\%SnO_2.1{,}0\%CoO.0{,}05\%Ta_2O_5.x\%Pr_6O_{11}$, em que x = 0,05, 0,10, 0,30 e 0,50% em mol. A dopagem com Pr_6O_{11} modifica o comportamento elétrico das cerâmicas. Os parâmetros elétricos encontrados foram: α = 8,0, E_B = 319 V cm^{-1} e V_b = 0,66 V $barreira^{-1}$ para o sistema ternário sem Pr_6O_{11} e α = 17,0, E_B = 853 V cm^{-1} e V_b = 1,15 V $barreira^{-1}$ para o sistema contendo 0,10% de Pr_6O_{11}. O sistema contendo 0.05% de Pr_6O_{11} apresentou o mesmo coeficiente não linear α que o sistema com 0,10%. Todavia, os valores obtidos de campo elétrico de ruptura e tensão, por barreira, foram menores (E_B = 708 V cm^{-1} e V_b = 0,98 V $barreira^{-1}$). Os baixos valores de campo elétrico de ruptura possibilitam o uso destes varistores para proteção em redes elétricas de baixa tensão. Para concentrações de Pr_6O_{11} acima de 0,10% em mol, a dopagem se torna deletério às propriedades elétricas do varistor. Tal efeito se deve ao aumento da concentração da fase estanato de praseodímio ($Pr_2Sn_2O_7$). Esta fase cristalina, juntamente com a fase cassiterita (SnO_2), foram encontradas por DRX e MEV/EDS e quantificadas por refinamento pelo método de Rietveld.

Palavras-chave: caracterização, dióxido de estanho, óxido de praseodímio, óxido de tântalo.

Introduction

Varistor ceramics are polycrystalline materials that present non-ohmic properties at certain working electric voltage range. They protect electrical circuits against over-voltages without being destroyed.

The quality of the protection offered by the varistor is given by the non-linearity coefficient (α) defined by the relation $I = c.V^{\alpha}$, where I is the current, V is the voltage and c is a proportionality constant.

The varistor ceramics present a semi-insulating characteristic (ohmic resistor) up to a certain voltage, called breakdown electric field (E_B), and start acting as an electrical conductor from this threshold. The breakdown electric field rate determines the use of a varistor ceramic in either high or low-voltage energy grids (MENEGOTTO et al., 2002).

SnO_2 is one of the frequently studied materials as a varistor ceramic since it provides monophasic varistors, unlike the ZnO polyphasic varistors.

Although pure SnO_2 presents intrinsic non-ohmic behavior and low densification, it may be used to produce a varistor system when properly doped.

Research works have been found in the literature in which dopants such as CoO and MnO densify SnO_2, while dopants such as Nb_2O_5 and Ta_2O_5 promote the electrical conductivity of SnO_2 (BUENO et al., 2004; MENEGOTTO et al., 2002; VARELA et al., 1999).

Specific literature (MENEGOTTO et al., 2002) shows that the addition of Cr_2O_3 to SnO_2.CoO.Ta_2O_5-based varistor increases the non-linear coefficient. The authors suggest that the effect of Cr_2O_3 is to produce higher and wider potential barriers at the SnO_2 grain boundaries. Other dopants with 3+ charges, such as Pr_2O_3, may be used to promote the formation of potential barrier in SnO_2-based varistor.

In current analysis the addition of Pr_6O_{11} to the ternary system SnO_2.1.0%CoO.0.05%Ta_2O_5 verified the influence of this oxide in potential barrier formation and in microstructure modifications.

Material and methods

Current analysis verified the influence of the Pr_6O_{11} dopant on the SnO_2.CoO.Ta_2O_5 ternary system. Pr_6O_{11} concentrations were 0.05, 0.10, 0.30 and 0.50 mol %, with concentration constants of CoO in 1.0 mol % and Ta_2O_5 in 0.05 mol %. The oxides employed were SnO_2 (CESBRA), Co_3O_4 (VETEC), Ta_2O_5 (ALDRICH), Pr_6O_{11} (ALDRICH) featuring analytical grade (purity ≥ 99.5 %).

Table 1 shows the compositions of the systems analyzed.

Table 1. Composition in molar percentage of the studied systems.

Varistor Systems	SnO_2 (mol %)	Co_3O_4 (mol %)	Ta_2O_5 (mol %)	Pr_6O_{11} (mol %)
Pr0	99.62	0.33	0.05	0.00
Pr0.05	99.57	0.33	0.05	0.05
Pr0.10	99.52	0.33	0.05	0.10
Pr0.30	99.32	0.33	0.05	0.30
Pr0.50	99.12	0.33	0.05	0.50

The systems were prepared by the conventional oxide mixture in Ball Mill, using zirconia balls as milling elements and isopropyl alcohol for wet homogenization. After milling, the powders were dried in an oven at 100°C $12h^{-1}$ and de-agglomerated in a 149 μm sieve (# 100 mesh). Samples were pressed to form pellets in an isostactic press at 50 MPa, with 10 mm diameter metallic molds. Samples were sintered at 1350°C $2h^{-1}$ at air atmosphere, with 10°C $min.^{-1}$ heating rate and 5°C $min.^{-1}$ cooling rate.

Samples sintered were analyzed through X-ray diffraction with phase quantification by Rietveld method. An X-ray diffractometer SHIMATZU XRD 6000 was used for this analysis, at θ-2θ configuration; KCuα tube operating in 40.0 kV and 30.0 mA; range $20^o \geq 2\theta \geq 120^o$; step 0.02^o; integration time of 4s $step^{-1}$; divergence slit 0.5^o; scatter slit 0.5^o; receiving slit 0.15 mm. Data were refined by Rietveld method.

Microstructural characterization was performed by scanning electron microscopy (SEM/EDS SHIMADZU SSX 550). The samples were ground, polished and thermally etched at 1300°C for 15 min. to reveal the microstructure. The mean grain size was measured following method by (MENDELSON, 1969).

For electrical characterization, a regulated voltage source was used (TECTRON TCH 3000-2) and the voltage (V) and current (I) readings carried out in digital multimeters (FLUKE 8050 A). The electrical measurements (I versus V) were performed in continuous current (CC) at various temperatures and normalized to J (density of current, mA cm^{-2}) x E (electric field, V cm^{-1}). The breakdown electric field (E_B) was determined at current density of 1 mA cm^{-2} and the leakage current (I_L) was determined at an electric field of 200 V cm^{-1}. The non-linearity coefficient α was obtained from the points in Log E as a function of Log J curve, for J values between 1 and 10 mA cm^{-2}.

Results and discussion

Figure 1 presents the XRD diffractograms of the non-doped SnO_2, Pr0 ternary system and Pr0.05, Pr0.10, Pr0.30, Pr0.50 quaternary systems, with different Pr_6O_{11} concentrations. As may be observed, only the diffraction peaks that refer to the cassiterite phase (JCPDF 41-1445) were identified for the ternary system Pr0. However, the existence of a spinel phase Co_2SnO_4 (cobalt stannate) in this system, at small concentrations non-detectable by XRD, already observed by other authors (MOREIRA et al., 2006; OLIVEIRA et al., 2003), cannot be ignored. The Pr_6O_{11} doped quaternary systems comprise two ceramic phases. As Figure 1 shows, the increase in the praseodymium oxide concentration in the composition was followed by an increase in the intensity of peaks ($2\theta \approx 29$ and 49^o) related to the $Pr_2Sn_2O_7$ pyrochlore phase (praseodymium stannate - JCPDF 13-0184). Phase $Pr_2Sn_2O_7$ has also been cited in literature for SnO_2-based varistors doped with CoO, Nb_2O_5 or Ta_2O_5

(OLIVEIRA et al., 2003; SAFAEE et al., 2011; WANG et al., 2005).

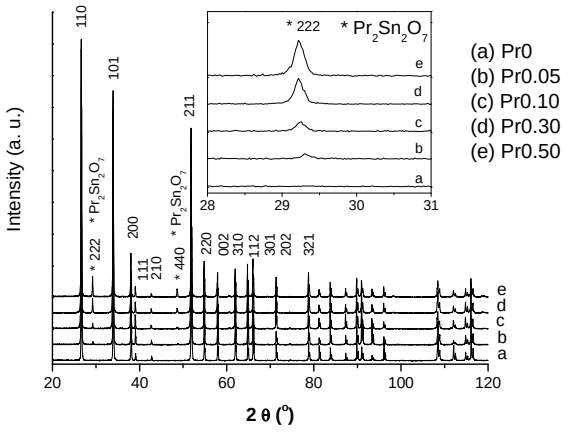

Figure 1. X-Ray diffractograms showing cassiterite (SnO_2) and $Pr_2Sn_2O_7$ phases characteristic peaks for the systems: (a) Pr0; (b) Pr0.05; (c) Pr0.10; (c) Pr0.30; (d) Pr0.50.

Cell parameters could be determined and the phases present could be identified and quantified from XRD refinement by the Rietveld method.

Table 2 shows results of the quantification of phases characterized by XRD by Rietveld method, cell parameters and Rietveld statistic indicators.

Through an increase in the compositions Pr_6O_{11} concentration, a decrease in the cassiterite phase (SnO_2) and an increase in the $Pr_2Sn_2O_7$ pyrochlore phase occurred. Table 2 reveals that a 10 times increase of Pr_6O_{11} concentration, from 0.05 % (Pr0.05) to 0.50 % in mol of Pr_6O_{11} (Pr0.50), a tenfold increase in the $Pr_2Sn_2O_7$ pyrochlore phase occurred, namely from 0.7 to 7.0%. The above indicated that nearly all the Pr_6O_{11} added to the composition was consumed in the formation of the pyrochlore phase.

The cell volume in the Pr0.05 system increased in relation to the Pr0 system. An increase in Pr_6O_{11} (Pr0.10 to Pr0.30) concentration caused a decrease in the cell volume. This was due to the release of Sn^{4+} ions from the cell interior to form the $Pr_2Sn_2O_7$ secondary phase.

Statistical indicators evaluated the quality of XRD data refinement by the Rietveld Method. The $S = R_{wp}/R_{exp}$ index must be a rate close to 1.0 so that the refinement may be considered good. The Bragg R factor, R_B, is related to the calculated structural model, indicating whether the model chosen represented well the real crystalline structure. Rates obtained in current research were relatively high due to the difficulty to model the structural disorder, microdeformations and the crystal size anisotropy, caused by the release of Sn^{4+} ions from the SnO_2 crystalline reticulum to form the $Pr_2Sn_2O_7$ secondary phase.

So that the morphology, distribution and chemical elements' distribution in the varistor ceramic microstructures could be characterized, SEM/EDS analyses were carried out. Figure 2a shows the micrography of the ternary system Pr0. The ternary system microstructure shows pores trapped inside the grains, few pores located in the grain boundaries, and the absence of precipitates related to the secondary phase $Pr_2Sn_2O_7$. Figure 2b registers the micrograph of the quaternary system Pr0.50. Drastic reduction in the average grain size is seen with the addition of Pr_6O_{11}. The presence of pores in the sintered systems may also be observed by the micrographs.

Figure 3 shows enlarged micrographs of the quaternary system Pr0.05, revealing the presence of precipitates in the triple junctions of the microstructure and inside the grains. These precipitates were ascribed to the $Pr_2Sn_2O_7$ secondary phase. Precipitate analysis by SEM/EDS chemical analysis identified grains with high concentration of Sn and Pr with regard to the $Pr_2Sn_2O_7$ phase. The above was identified by XRD as well as grains with high concentration of Sn and Co that might be related to the solid solution between cobalt and tin oxides or, with the spinel Co_2SnO_4 (cobalt stannate) phase, which, although not identified by XRD in current analysis, were probably present in small amounts in the microstructure, as pointed out by other authors (MOREIRA et al., 2006; OLIVEIRA et al., 2003; VARELA et al., 1999).

Table 2. Rietveld quantification of phases characterized by XRD.

Varistor Systems	Quantified Phases	Cell Parameters				Rietveld Statistic Indicators			
		a (Å)	c (Å)	c / a	V (Å^3)	R_{wp} (%)	R_{exp} (%)	S	R_B
Pr0	100 % SnO_2	4.73758(5)	3.18647(5)	0.67259(4)	71.519(2)	20.97	10.98	1.91	11.90
Pr0.05	99.3 % SnO_2 + 0.7 $Pr_2Sn_2O_7$	4.73762(3)	3.18664(3)	0.67265(3)	71.527(1)	17.14	10.32	1.66	6.89
Pr0.10	98.6 % SnO_2 + 1.4 $Pr_2Sn_2O_7$	4.73748(3)	3.18644(3)	0.67260(2)	71.515(1)	17.02	10.54	1.61	6.53
Pr0.30	96.0 % SnO_2 + 4.0 $Pr_2Sn_2O_7$	4.73719(3)	3.18642(3)	0.67264(2)	71.506(1)	14.81	11.07	1.33	3.84
Pr0.50	93.0 % SnO_2 + 7.0 $Pr_2Sn_2O_7$	4.7370(3)	3.1864(3)	0.67265(2)	71.501(1)	14.09	10.87	1.29	3.84

Precipitates of $Pr_2Sn_2O_7$ phase in the grain boundaries caused grain growth inhibition by pinning process leading to a decrease in average grain size.

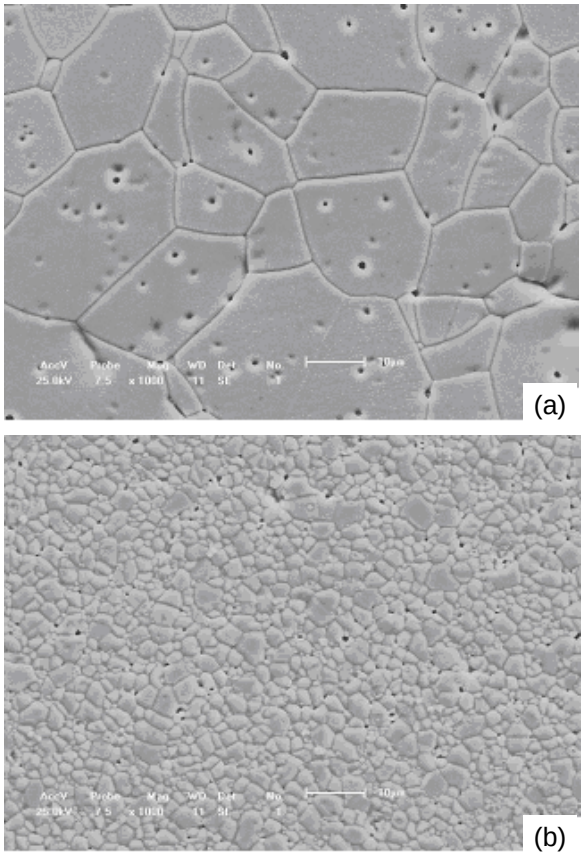

Figure 2. SEM-obtained micrographs of the compact ceramic systems (a) Pr0 and (b) Pr0.50, sintered at 1350ºC $2h^{-1}$. Magnified 1000 X.

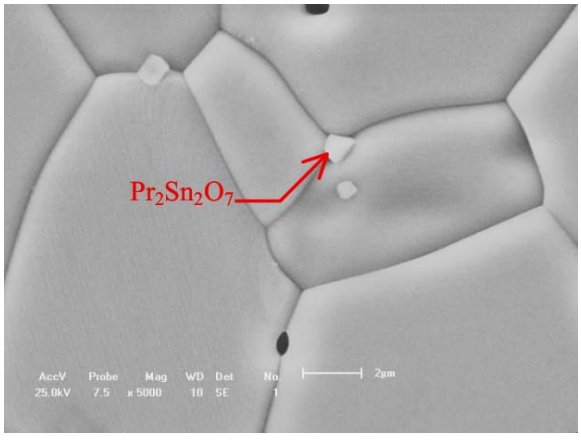

Figure 3. SEM-obtained micrographs of the quaternary ceramic systems Pr0.05, sintered at 1350ºC $2h^{-1}$. Magnified 5000 X.

Average grain sizes were calculated by Equation (1), in which d is the average grain size; n is the number of grains intercepted by a test line with known L (μm) length (MENDELSON, 1969).

$$d = 1.558\frac{L}{n} \quad (1)$$

Table 3 shows average grain size obtained by the systems. Data analysis reveals the drastic reduction in the average grain size, from 20.8 μm in the ternary system Pr0 to 4.3 μm, when Pr_6O_{11} concentration reached 0.50% (in mol) in the Pr0.50 system. The presence of precipitates of the secondary phase $Pr_2Sn_2O_7$ led to a maximum decrease of 5 times the average grain size when compared to that of the ternary system. Reduction effect in the average grain size due to the Pr_6O_{11}doping has also been verified by other authors in the literature (OLIVEIRA et al., 2003; SAFAEE et al., 2011; SIMÕES et al., 2003; WANG et al., 2005; ZHANG et al., 2007) and is also related with the grain growth inhibition caused by the presence of secondary phase precipitates in the grain boundaries.

Table 3. Average grain size obtained for the systems.

Varistor Systems	Average Grain Size (μm)
Pr0	20.8
Pr0.05	13.9
Pr0.10	13.4
Pr0.30	5.8
Pr0.50	4.3

The average grain size rates obtained in current research were three times larger than those reported in the literature for similar systems (SIMÕES et al., 2003). This was due to the higher sintering temperature in the assay. Equation (2) demonstrates that larger grain sizes (d) lead to a decrease in the number of effective barriers (N_b) present in the varistor ceramics, considering a fixed thickness (t) of the sample, for example, 1mm. Equation (3) reveals that the reduction in the number of effective barriers (N_b) leads to a decrease in its breakdown electric field (E_B), favoring the use of such varistors in low-voltage energy grids.

$$N_b = \frac{t}{d} \quad (2)$$

The accumulation of positive punctual defects in the grain boundaries region and negative defects in the grain-grain interface leads to the formation of the potential barrier responsible for the varistor effect in SnO_2-based ceramics. The varistor effect of such ceramics may be verified by performing electric measurements in continuous current.

In Figure 4, the characteristic curves (E versus J) of the systems, measured at room temperature, are

given. The systems Pr0, Pr0.05, Pr0.10, Pr0.30 presented non-linear electrical behavior, typical of varistor systems. The system Pr0.50 provided a linear electrical behavior within the range of current and voltage studied.

It is known that the electrical properties of varistors are strongly influenced by the temperature and the presence of applied electrical field. In Figure 5, the Ln E versus Ln J characteristic curves carried out at different temperatures for the quaternary system Pr0.05 are presented. In Figure 5, strong influence of temperature on the varistor properties may be observed, indicating Schottky-type thermally activated electrical conduction. The same behavior was observed in other systems under analysis.

The values of electrical (E_B, α, I_L) and potential barrier (V_b, ϕ_b, β) parameters are given in Table 4. The V_b values were obtained from Equation (3).

$$V_b = \frac{E_B}{N_b} \quad (3)$$

where V_b is the voltage per barrier at the grain boundary, E_B is the breakdown electrical field and N_b is the number of effective barriers (Equation 2). Height and width of potential barrier may be determined from electrical measurements (I x V) at several temperatures (Figure 5) and taking into consideration the Schottky-type conduction model (Equations 4 and 5). Using the linear region of graphs ln J as a function of $\sqrt{E}$, the β (related to the potential barrier width – Equation 5) rate is obtained and from the slope of graphs ln J as a function of 1/T, the ϕ_b (potential barrier height – Equation 4) rates are obtained. Height ϕ_b and parameter β potential barrier for the systems Pr0-Pr0.10, which presented a good varistor behavior, are shown in Table 4.

$$J_s = A^* T^2 e^{\frac{-(\phi_b - \beta\sqrt{E})}{kT}} \quad (4)$$

where: $A^\star$ is the Richardson constant, T is the absolute temperature, ϕ_b the potential barrier height, E is the applied electrical field, and k is the Boltzmann constant. Parameter β is inversely proportional to the square root of the potential barrier width (ω):

$$\beta = \left[\left(\frac{1}{N_b \omega}\right)\left(\frac{e^3}{4\pi\varepsilon_0\varepsilon_r}\right)\right]^{\frac{1}{2}} \quad (5)$$

where N_b is the number of effective barriers (Equation 2), e is the elementary electrical charge, ε_0 and ε_r are vacuum electric permittivity and material electric permittivity respectively.

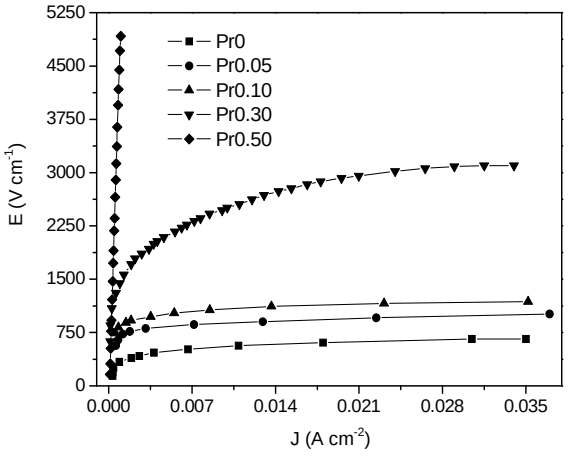

Figure 4. Electrical Field (E) according to the current density (J) of the systems Pr0, Pr0.05, Pr0.10, Pr0.30 and Pr0.50, sintered at 1350°C $2h^{-1}$.

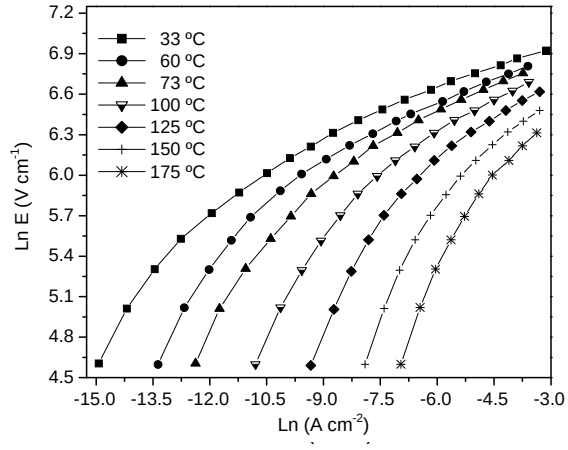

Figure 5. Ln E versus Ln J characteristic curves at different temperatures for the system Pr0.05, sintered at 1350°C $2h^{-1}$.

Table 4. Electrical and potential barrier parameters obtained for the systems.

Varistor Systems	E_B (V cm^{-1})	α	I_L† (A)	V_b (V $barrier^{-1}$)	ϕ_b (eV)	β ($V^{1/2}$ $cm^{1/2}$) x 10^3
Pr0	319	8.0	1.55 x 10^{-4}	0.66	0.27	15.57
Pr0.05	708	17.0	7.11 x 10^{-5}	0.98	0.69	9.64
Pr0.10	853	17.0	7.11 x 10^{-5}	1.15	0.75	8.52
Pr0.30	1608	8.6	6.92 x 10^{-5}	0.92	-	-
Pr0.50	-	-	-	-	-	-

† I_L at 200 V cm^{-1}.

There is an increase in the breakdown electric field value (E_B) with an increase in the Pr_6O_{11} concentration. The E_B value increased almost 5 times with the increase in Pr_6O_{11} from Pr0 to Pr0.30 systems. System Pr0.50 presented a linear

electrical behavior in the range of current and voltage studied. Such increase in E_B is related in Equations (2 and 3) with the reduction in the average grain size (d) verified through the SEM microstructural characterizations (Figure 2 and Table 3). For constant values of V_b and sample thickness (t), a reduction in the average grain size (d) leads to an increase in the number of effective barrier (N_b) present in grain boundaries, with a consequent increase in E_B value. However, E_B rates obtained in this work for systems Pr0.05 and Pr0.10 are about 7 times lower than those reported in the literature for similar systems (SIMÕES et al., 2003), favoring the use of such ceramics in low-voltage energy grids.

A significant reduction in the leakage current (I_L) with an increase in Pr_6O_{11} concentration was also observed. The leakage current reduction is due to the higher resistivity caused by reduction in average grain size (Table 3) with an increase in Pr_6O_{11} concentration.

The increase in the Pr_6O_{11} concentration also leads to an increase in the non-linearity coefficient from $\alpha = 8.0$ in the ternary system Pr0 to $\alpha = 17.0$ in the quaternary systems Pr0.05 and Pr0.10. These results show that Pr_6O_{11} promoted the varistor effect in these ceramics. For the system Pr0.30, the non-linearity coefficient rate was drastically reduced and for the system Pr0.50, the E versus J response was linear in the range of current and voltage studied, which did not correspond to a varistor behavior. Thus, a maximum limit value of 0.10 % in mol of Pr_6O_{11} may be considered the limit value for the systems under analysis. Above this concentration, their effect becomes deleterious for varistor characteristics. This limit is related to Pr_6O_{11} solubility in the SnO_2 matrix, where the increase in the concentration above 0.10% in mol Pr_6O_{11} leads to the formation of great amounts of the secondary phase $Pr_2Sn_2O_7$.

The V_b value increased in relation to the ternary system Pr0. This indicated that Pr_6O_{11} contributed to the formation of potential barriers at the grain boundaries, similarly to Cr_2O_3, as described by (MENEGOTTO et al., 2002). The V_b values obtained for the Pr_6O_{11} doped systems Pr0.05, Pr0.10 and Pr0.30 were nearly the same, even with the increase in the dopant concentration. This indicated that the E_B increase in relation to system Pr0 was mainly due to the effect of the reduction in the average grain size caused by the increase in the dopant Pr_6O_{11} content, as discussed above.

Table 4 shows an increase in the potential barrier height ϕ_b and a decrease in the β parameter, which represents increase in the potential barrier width with Pr_6O_{11} addition to the ternary system Pr0. This fact is in accordance with results obtained in the electrical characterization, where increase in E_B and α is observed (Table 4), since such electrical properties are affected by the potential barrier present in the grain boundaries.

Changes in the potential barrier may be explained by the segregation in the region of grain boundaries of point defects due to the Pr_6O_{11} solid solution formation, in addition to the solid solution formed with Ta_2O_5 and CoO/Co_2O_3 in SnO_2, according to the equations:

++

$$Pr_2O_3 \xrightarrow{SnO_2} 2\,Pr_{Sn}^{'} + V_O^{\cdot\cdot} + 3\,O_O^x \quad (6)$$

$$2\,Ta_2O_5 \xrightarrow{SnO_2} 2\,Ta_{Sn}^{\cdot} + V_{Sn}^{''''} + 10\,O_O^x \quad (7)$$

$$CoO \xrightarrow{SnO_2} Co_{Sn}^{''} + V_O^{\cdot\cdot} + O_O^x \quad (8)$$

$$Co_2O_3 \xrightarrow{SnO_2} 2\,Co_{Sn}^{'} + V_O^{\cdot\cdot} + 3\,O_O^x \quad (9)$$

The increase in the potential barrier may also be associated with the increase in effective surface states (N_s), according to the following equation:

$$\phi_b = \frac{e^2 N_s^2}{2\varepsilon_0 \varepsilon_r N_d} \quad (10)$$

Increase in the potential barrier height and width are then associated with the increase in both N_s and N_d (density of donors) due to the segregation of Pr_2O_3 next to the grain boundaries as well as to the creation of positive defects ($V_O^{\cdot\cdot}$) in the depletion layer and negative defects at the grain-grain interface (Pr_{Sn}'). After the adsorption of oxygen from atmosphere at the grain-grain interface and the transfer of negative charges from (Pr_{Sn}') and other negative species to the adsorbed oxygen, which increases N_s. Considering the SnO_2 varistor microstructure, a Schottky-type electrical barrier may be ascribed as the most likely barrier at the SnO_2 grain boundary, since no inter-granular insulating layer separating two SnO_2 grains was observed in SEM. The negative surface charge at the grain boundary interface is compensated by the positive charge in the depletion layer in the grain on both sides of the grain-grain interface (GUPTA; CARLSON, 1985) developed a grain boundary defect model comprising the Schottky barrier.

In an attempt to explain the grain boundary barrier formation in a SnO_2 varistor, an analogy to this model may be considered, as Figure 6 demonstrates. In this model, the intrinsic SnO_2 defects ($V_{Sn}^{''''}$, $V_O^{\cdot\cdot}$) and extrinsic defects created by the dopants CoO/Co_2O_3; Ta_2O_5 and Pr_6O_{11} could be responsible for the grain boundary electrical barrier formation. These dopants form a solid solution with the SnO_2 at high temperatures and create defects near the grain boundary, according to Equations 6 to 9.

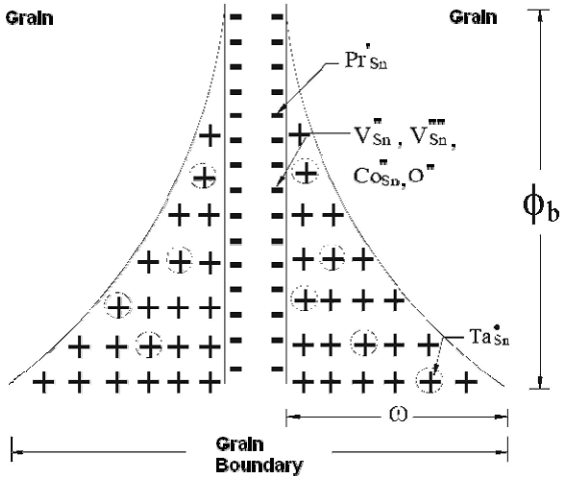

Figure 6. Atomic defect model proposed to the formation of a potential barrier in the grain boundaries with the addition of Pr_6O_{11} to the SnO_2.CoO.Ta_2O_5 systems.

In Figure 6, positively charged donors ($V_O^{\cdot\cdot}$, $Ta_{Sn}^{\cdot}$), extending from both sides of the grain boundary, are compensated by negative charged acceptors ($V_{Sn}^{''''}$, $V_{Sn}^{''}$, Co_{Sn}', Co_{Sn}'', Pr_{Sn}') at the grain-grain interface. The oxygen could also be responsible for Schottky barrier formation if oxygen is adsorbed at the grain-grain interface and reacts with negative defects, according to the following equations:

$$O_2 \rightarrow O^x_{2(ads)} \quad (11)$$

$$V''''_{Sn} + 4O^x_{2(ads)} \rightarrow V^x_{Sn} + 4O'_{2(ads)} \quad (12)$$

$$V''''_{Sn} + 2O^x_{2(ads)} \rightarrow V''_{Sn} + 2O'_{2(ads)} \quad (13)$$

$$V''_{Sn} + 2O'_{2(ads)} \rightarrow V^x_{Sn} + 4O'_{(ads)} \quad (14)$$

$$Co''_{Sn} + 2O^x_{2(ads)} \rightarrow Co^x_{Sn} + 2O'_{2(ads)} \quad (15)$$

$$Pr'_{Sn} + O^x_{2(ads)} \rightarrow Pr^x_{Sn} + O'_{2(ads)} \quad (16)$$

$$Pr'_{Sn} + O'_{2(ads)} \rightarrow Pr^x_{Sn} + 2O'_{(ads)} \quad (17)$$

The absorbed oxygen at the grain boundary captures electrons from negatively charged defects at the grain boundary and remains at the grain-grain interface, modifying the potential barrier and consequently the electrical properties of varistor systems.

Conclusion

The detection of a secondary phase $Pr_2Sn_2O_7$, present in all quaternary systems was possible by XRD and SEM/EDS techniques. The reduction in grain average size was due to the growth inhibition process caused by the precipitates of $Pr_2Sn_2O_7$ in the grain boundaries. All compositions under study, except that containing 0.50% in mol Pr_6O_{11}, presented non-linear electrical behavior, with significant decrease in the leakage current and increase in the breakdown electrical field. The breakdown electric field rates obtained indicated that varistor systems were suitable for the protection of low-voltage energy grids.

Acknowledgements

The authors would like to thank CNPq, CAPES/PNPD and Fundação Araucária, Paraná State, Brazil for their financial support and funding.

References

BUENO, P. R.; ORLANDI, M. O.; SIMÕES, L. G. P.; LEITE, E. R.; LONGO, E.; CERRI, J. A. Nonohmic behavior of SnO_2-MnO polycrystalline ceramics. I. Correlations between microstructural morphology and nonohmic features. **Journal of Applied Physics**, v. 96, n. 5, p. 2693-2701, 2004.

GUPTA, T. K.; CARLSON, W. G. A grain-boundary defect model for instability/stability of a ZnO varistor. **Journal of Materials Science**, v. 20, n. 10, p. 3487-3500, 1985.

MENDELSON, M. I. Average Grain Size in Polycrystalline Ceramics. **Journal of the American Ceramic Society**, v. 52, n. 8, p. 443-446, 1969.

MENEGOTTO, G. F.; PIANARO, S. A.; ZARA, A. J.; ANTUNES, S. R. M.; ANTUNES, A. C. J. Varistor behavior of the system SnO_2.CoO.Ta_2O_5.Cr_2O_3. **Journal of Materials Science. Materials in Electronics**, v. 13, n. 5, p. 253-256, 2002.

MOREIRA, M. L.; PIANARO, S. A.; ANDRADE, A. V. C.; ZARA, A. J. Crystal phase analysis of SnO_2-based varistor ceramic using the Rietveld method. **Materials Characterization**, v. 57, n. 3, p. 193-198, 2006.

OLIVEIRA, M. M.; SOARES JR.; P. C.; BUENO, P. R.; LEITE, E. R.; LONGO, E.; VARELA, J. A. Grain-boundary

segregation and precipitates in La_2O_3 and Pr_2O_3 doped SnO_2·CoO-based varistors. **Journal of the European Ceramic Society**, v. 23, n. 11, p. 1875-1880, 2003.

SAFAEE, I.; BAHREVAR, M. A.; SHAHRAKI, M. M.; BAGHSHAHI, S.; AHMADI, K. Microstructural characteristics and grain growth kinetics of Pr_6O_{11} doped SnO_2-based varistors. **Solid State Ionics**, v. 189, n. 1, p. 13-18, 2011.

SIMÕES, G. P.; ORLANDI, M. O.; ARAUJO, A. L.; BOMIO, M. R. D.; LEITE, E. R.; LONGO, E.; VARELA, J. A. Efeito do Pr_2O_3 nas propriedades elétricas de varistores à base de SnO_2. **Cerâmica**, v. 49, n. 312, p. 232-236, 2003.

VARELA, J. A.; CERRI, J. A.; LEITE, E. R.; LONGO, E. M.; SHAMSUZZOHAC, R. C.; BRADT, C. Microstructural evolution during sintering of CoO doped SnO_2 ceramics. **Ceramics International**, v. 25, n. 3, p. 253-256, 1999.

WANG, J. F.; SU, W. B.; CHEN, H. C.; WANG, W. X.; ZANG, G. Z.; LI, C. P.; BODDE, S. (Pr, Co, Nb)-doped SnO_2 varistor ceramics. **Journal of the American Ceramic Society**, v. 88, n. 2, p. 331-334, 2005.

ZHANG, C. J.; WANG, J. F.; SU, W. B.; ZANG, G. Z.; CHEN, H. C. Grain size effects of SnO_2 varistor induced by doping Pr. **Key Engineering Materials**, v. 280-283, n. 1, p. 275-278, 2007.

Received on July 19, 2012.
Accepted on June 10, 2013.